with lung adenocarcinoma.	K., Schetter AJ., Ogata-Kawata H., Tsuchiya N., Kunitoh H., Nokihara H., Watanabe S., Tsuta K., Kumamoto K., Takenoshita S., Yokota J., Harris CC., Kohno T			
NEK9-dependent proliferation of cancer cells lacking functional p53.	Kurioka D., Takeshita F., Tsuta K., Sakamoto H., Watanabe S., Matsumoto K., Watanabe M., Nakagama H., Ochiya T., Yokota J., Kohno T., Tsuchiya N	Sci Rep. 4, 6111. 2014	2014年8月	国外
Circulating Exosomal microRNAs as Biomarkers of Colon Cancer.	Ogata-Kawata H, Izumiya M, Kurioka D, Honma Y, Yamada Y, Furuta K, Gunji T, Ohta H, Okamoto H, Sonoda H, Watanabe M, Nakagama H,	PLoS ONE 9: e92921. 2014	2014年4月	国外

	Yokota J, Kohno T, Tsuchiya N			
A Rare Polymorphic Variant of NBS1 Reduces DNA Repair Activity and Elevates Chromosomal Instability.	Yamamoto Y, Miyamoto M, Tatsuda D, Kubo M, Nakagama H, Nakamura Y, Satoh H, Matsuda K, Watanabe T, Ohta T	Cancer Res. 2014 Jul;74(16):3707-3715.	2014年7月	国外
Clinical relevance and therapeutic significance of microRNA-133a expression profiles and functions in malignant osteosarcoma-initiating cells.	Fujiwara T, Katsuda T, Hagiwara K, Kosaka N, Yoshioka Y, Takahashi RU, Takeshita F, Kubota D, Kondo T, Ichikawa H, Yoshida A, Kobayashi E, Kawai A, Ozaki T, Ochiya T.	Stem Cells. 2014 Apr.32(4):959-73.	2014年4月	国外
Phase I and pharmacokinetic study of trabectedin, a DNA minor groove binder, administered as a 24-h continuous infusion in Japanese patients with	Ueda T, Kakunaga S, Ando M, Yonemori K, Sugiura H, Yamada K, Kawai A.	Invest New Drugs. 2014 Aug;32(4):691-9.	2014年8月	国外

soft tissue. sarcoma				
STAT6 immunohistochemistry is helpful in the diagnosis of solitary fibrous tumors.	Yoshida A, Tsuta K, Ohno M, Yoshida M, Narita Y, Kawai A, Asamura H, Kushima R.	Am J Surg Pathol. 2014 Apr;38(4):552-9.	2014年4月	国外
International expert opinion on patient-tailored management of soft tissue sarcomas.	Blay JY, Sleijfer S, Schöffski P, Kawai A, Brodowicz T, Demetri GD, Maki RG.	Eur J Cancer. 2014 Mar;50(4):679-89.	2014年3月	国外
MicroRNA expression and functional profiles of osteosarcoma.	Kobayashi E, Satow R, Ono M, Masuda M, Honda K, Sakuma T, Kawai A, Morioka H, Toyama Y, Yamada T.	Oncology. 2014;86(2):94-103.	2014年1月	国外
SS18-SSX fusion protein-induced Wnt/β-catenin signaling is a therapeutic target in synovial sarcoma.	Trautmann M, Sievers E, Aretz S, Kindler D, Michels S, Friedrichs N, Renner M, Kirfel J, Steiner S, Huss S, Koch A, Penzel R, Larsson O,	Oncogene. 2014 Oct 16;33(42):5006-16.	2014年10月	国外

	Kawai A,			
RPN2 Gene Confers Osteosarcoma Cell Malignant Phenotypes and Determines Clinical Prognosis.	Fujiwara T, Takahashi RU, Kosaka N, Nezu Y, Kawai A, Ozaki T, Ochiya T.	Mol Ther Nucleic Acids. 2014 Sep 2;3:e189.	2014年9月	国外
Multiple metastases from histologically benign intraarticular diffuse-type tenosynovial giant cell tumor: a case report.	Asano N, Yoshida A, Kobayashi E, Yamaguchi T, Kawai A.	Hum Pathol. 2014 Nov;45(11):2355-8.	2014年11月	国外
Unique mutation portraits and frequent COL2A1 gene alteration in chondrosarcoma.	Totoki Y, Yoshida A, Hosoda F, Nakamura H, Hama N, Ogura K, Yoshida A, Fujiwara T, Arai Y, Toguchida J, Tsuda H, Miyano S, Kawai A, Shibata T.	Genome Res. 2014 Sep;24(9):1411-20.	2014年9月	国外

Ⅳ．研究成果の刊行物・別刷

Cancer Science
Japanese Cancer Association JCA
Open Access

Prognostic significance of promyelocytic leukemia expression in gastrointestinal stromal tumor; integrated proteomic and transcriptomic analysis

Hiroshi Ichikawa,[1,2] Akihiko Yoshida,[3] Tatsuo Kanda,[4] Shin-ichi Kosugi,[2] Takashi Ishikawa,[2] Takaaki Hanyu,[2] Takahiro Taguchi,[5] Marimu Sakumoto,[1] Hitoshi Katai,[6] Akira Kawai,[7] Toshifumi Wakai[2] and Tadashi Kondo[1]

[1]Division of Pharmacoproteomics, National Cancer Center Research Institute, Tokyo; [2]Division of Digestive and General Surgery, Niigata University Graduate School of Medical and Dental Sciences, Niigata; [3]Department of Pathology and Clinical Laboratories, National Cancer Center Hospital, Tokyo; [4]Department of Surgery, Sanjo General Hospital, Niigata; [5]Research and Education Faculty, Multidisciplinary Science Cluster, Kuroshio Science Unit, Kochi; [6]Division of Surgical Oncology, National Cancer Center Hospital, Tokyo; [7]Division of Musculoskeletal Oncology, National Cancer Center Hospital, Tokyo, Japan

Key words

Gastrointestinal stromal tumor, promyelocytic leukemia, proteomics, transcriptomics, tumor site

Correspondence

Tadashi Kondo, Division of Pharmacoproteomics, National Cancer Center Research Institute, 5-1-1 Tsukiji, Chuo-ku, Tokyo 104-0045, Japan.
Tel: +81-3-3542-2511 ext. 3004; Fax: +81-3547-5298;
E-mail: takondo@ncc.go.jp

Funding Information

This work was supported by the National Cancer Center Research Core Facility and the National Cancer Center Research and Development Fund (23-A-7 and 23-A-10).

Received August 15, 2014; Revised October 15, 2014; Accepted October 18, 2014

Cancer Sci **106** (2015) 115–124

doi: 10.1111/cas.12565

Prognostic markers are urgently needed to optimize the postoperative treatment strategies for gastrointestinal stromal tumors (GIST). GIST of the small intestine (I-GIST) show more aggressive behavior than those of the stomach (S-GIST), and the molecular background of the malignancy in I-GIST may include potential prognostic biomarkers. We conducted integrated proteomic and transcriptomic analysis to identify genes showing differential expressions according to the tumor site. We generated protein expression profiles for four cases each of surgically resected I-GIST and S-GIST using label-free proteomic analysis. For proteins showing differential expressions, global mRNA expression was compared between 9 I-GIST and 23 S-GIST. Among the 2555 genes analyzed, we found that promyelocytic leukemia (*PML*), a tumor suppressor gene, was significantly downregulated in I-GIST at both the protein and mRNA levels ($P < 0.01$; fold difference ≥2.0). Immunohistochemistry of 254 additional cases from multiple clinical facilities showed that PML-negative cases were significantly frequent in the I-GIST group ($P < 0.001$). The 5-year recurrence-free survival rate was significantly lower in the PML-negative than in the PML-positive cases (60.1% *vs* 91.7%; $P < 0.001$). Multivariate analysis revealed that downregulation of PML was an independent unfavorable prognostic factor (hazard ratio = 2.739; $P = 0.001$). Our study indicated that prognostication based on PML expression may have potential for optimizing the treatment strategy for GIST patients. Further validation studies of PML for clinical application, and investigation for the mechanistic significance of PML to clarify the molecular backgrounds of malignancy in GIST are warranted.

Gastrointestinal stromal tumors (GIST) are a common type of soft-tissue sarcoma.[1] Approximately 75–80% of GIST harbor an activating mutation in the *KIT* oncogene and 5–8% in platelet-derived growth factor receptor-α (*PDGFRA*), which are both key molecular drivers of GIST pathogenesis.[2–5] Adjuvant therapy with imatinib, a tyrosine kinase inhibitor, prolongs recurrence-free survival (RFS) after complete resection.[6,7] Recently, a randomized trial revealed that patients with a high-risk of recurrence show longer survival with 3 years of imatinib administration than with 1 year.[8] Almost all patients receiving imatinib therapy suffer some adverse effects, and approximately 50% of the operative GIST patients are cured by surgery alone.[8] Therefore, prognostic markers are needed to optimize adjuvant imatinib therapy.[9]

Gastrointestinal stromal tumor arise predominantly in the stomach (60–70%) and small intestine (20–30%).[10] GIST of the small intestine (I-GIST) show more aggressive behavior than those of the stomach (S-GIST), with similar size and mitotic activity.[11] Therefore, the tumor site is included as a factor in currently employed risk stratification schemes.[12] Investigations of genetic aberrations that are specific to tumors arising at certain anatomical sites can provide clues to understanding the molecular mechanisms of malignant behavior of GIST, thus leading to the development of prognostic biomarkers. It has been reported that differences in expression or mutation of *KIT* and *PDGFRA* are associated with the tumor site.[13,14] In addition, chromosomal aberrations and gene expressions that are specific to I-GIST have been identified in genome-wide global studies, and these have also been shown to be adverse prognostic factors.[15–20] However, these reports lack validation studies for the confirmation of the prognostic value and clinical utility. Therefore, intensive validation studies, including multi-institutional research, are needed to establish the prognostic biomarkers from tumor site-specific genes.

In the present study, we aimed to identify the molecular backgrounds specific to the tumor site and to discover the prognostic biomarker in GIST. We integrated proteomic and transcriptomic analysis, and observed a total of 2555 genes. For the proteomic analysis, we applied a label-free proteomics, allowing comprehensive analysis of thousands of proteins

using a combination of SDS-PAGE and mass spectrometry without isotopic labeling.[21–23] For the transcriptomic analysis, we used publicly available transcriptomic data for GIST. We identified 18 genes whose expressions differed between S-GIST and I-GIST at both the protein and mRNA levels. Among the 18 genes, we found that promyelocytic leukemia (*PML*), a tumor suppressor gene, was significantly downregulated in I-GIST and S-GIST that showed postoperative recurrence. Finally, using immunohistochemistry, we validated the prognostic utility of PML in 254 additional cases of GIST from multiple clinical facilities.

Patients and Methods

Patients and clinical information. We examined tumor tissues from 164 GIST patients who underwent surgery at the National Cancer Center Hospital between July 1972 and December 2005. Fresh frozen tumor tissues from 8 GIST patients were used for proteomic analysis. The mutational status of the *KIT* and *PDGFRA* was determined as described previously,[24] and the clinicopathological data for the individual patients are summarized in Table 1. Formalin-fixed paraffin-embedded (FFPE) tissue sections from 156 other GIST cases were examined immunohistochemically for independent validation (Suppl. Table S1). We also immunohistochemically examined 98 GIST cases that underwent surgery at Niigata University Hospital between October 1982 and December 2005 (Suppl. Table S2). All patients underwent resection with curative intent, and did not receive either neoadjuvant or adjuvant therapy with imatinib. Diagnosis was based on the World Health Organization Classification of Tumors of the Digestive System,[25] including tumor size, mitotic rate, presence of epithelioid morphology, and expression of CD34 and KIT. Recurrence risk was classified according to the NIH consensus criteria based on tumor size and mitotic count.[26] This project was approved by the institutional review boards of the National Cancer Center and Niigata University.

Label-free proteomic analysis. Proteins were extracted from fresh frozen tissues as described previously.[24] Sixty microgram protein samples were separated by 12.5% SDS-PAGE. Each gel lane was cut into 24 pieces of equal size using a GridCutter (Gel Company, San Francisco, CA, USA), and each gel piece was subjected to in-gel tryptic digestion as described previously.[27] The final trypsin digests were subjected to liquid chromatography coupled with LTQ-Orbitrap XL mass spectrometer (Thermo Fisher Scientific, San Jose, CA, USA) (Fig. 1a). Peptide identification and protein quantification were performed using Mascot (version 2.2; Matrix Science, London, UK) and Progenesis LC-MS version 3.4 (Nonlinear Dynamics, Newcastle, UK), respectively. Details of the mass spectrometric analysis are provided in the supporting information (Suppl. Doc. S1). The processed raw data for protein abundance was loaded to Expressionist analyst (GeneData, Basel, Switzerland), and subjected to quantile normalization, hierarchical clustering analysis, principal component analysis and statistical analysis using Welch's *t*-test.

Transcriptomic analysis. A publicly available microarray dataset (GSE8167), which had been previously generated using GeneChip Human Genome U133 Plus 2.0 arrays (Affymetrix, Santa Clara, CA, USA),[20] was obtained from the NCBI GEO database. The clinicopathological data for the 32 analyzed samples are summarized in Supplementary Table S3. Downloaded CELL files were imported into GeneSpring GX version 11.0 (Agilent Technologies, Santa Clara, CA, USA), and background correction, probe summarization and normalization were performed according to the RMA algorithm.[28] From the total of 54 675 probes, we extracted 6146 corresponding to the genes that had been observed in proteomic analysis. These probes were filtered according to the percentile of their signal intensities in the raw data (20-100th percentile). Among the remaining 6004 probes, hierarchical clustering analysis, principal component analysis, and statistical analysis using unpaired *t*-test with Benjamini and Hochberg's correction were performed (Fig. 1a).

Western blotting. Five microgram protein samples extracted from fresh frozen tumor tissues were separated by 12.5% SDS-PAGE and subsequently transferred to PVDF membranes. The separated proteins were reacted with a primary antibody against PML (1:500; Abcam, Cambridge, UK) at room temperature for 1 h, followed by a secondary antibody against rabbit IgG (1:2000; GE Healthcare Biosciences, Uppsala, Sweden) under the same conditions. The immune complex was detected by ECL Prime (GE Healthcare Biosciences) and LAS-3000 (Fuji Photo Film, Tokyo, Japan). The intensity of PML bands was normalized by that of the corresponding total lanes stained with Ponceau S using ImageQuant (GE Healthcare Biosciences).

Immunohistochemistry. Promyelocytic leukemia expression was examined immunohistochemically using FFPE tissues, as described in our previous report.[24] In brief, 4-μm-thick tissue sections were autoclaved in 10 mmol/L citrate buffer (pH 6.0) at 121°C for 30 min and incubated with the antibody against PML (1:500; Abcam) at room temperature for 1 h. Immunostaining was carried out by the streptavidin–biotin peroxidase method using the Strept ABC Complex/HRP kit (Dako, Glostrup, Denmark). One pathologist (A.Y.) and one clinician (H.I.), both blinded to the clinical data, reviewed the sections stained with anti-PML antibody. Tumor cells were

Table 1. Clinicopathological characteristics of the samples used in the proteomic analysis

Sample number	Anatomical tumor site	Gene mutation type	Histologic subtypes	Size (cm)	Mitosis (/50 HPF)	Risk classification†	Recurrence
1	Stomach	Wild type of *KIT* and *PDGFRA*	Spindle	3.5	≤5	Low	Absence
2	Stomach	Wild type of *KIT* and *PDGFRA*	Spindle	4.0	≤5	Low	Absence
3	Stomach	*KIT* exon 11 deletion	Mixed	12.0	>10	High	Peritoneum
4	Stomach	*KIT* exon 11 deletion	Mixed	4.0	>10	High	Liver
5	Small intestine	*KIT* exon 9 insertion	Spindle	3.7	≤5	Low	Absence
6	Small intestine	*KIT* exon 11 deletion	Spindle	7.0	≤5	Intermediate	Absence
7	Small intestine	*KIT* exon 11 deletion	Spindle	18.0	6–10	High	Liver
8	Small intestine	*KIT* exon 9 deletion	Mixed	7.0	>10	High	Peritoneum

†Recurrence risk was classified according to NIH consensus criteria. HPF, high power field of the microscope.

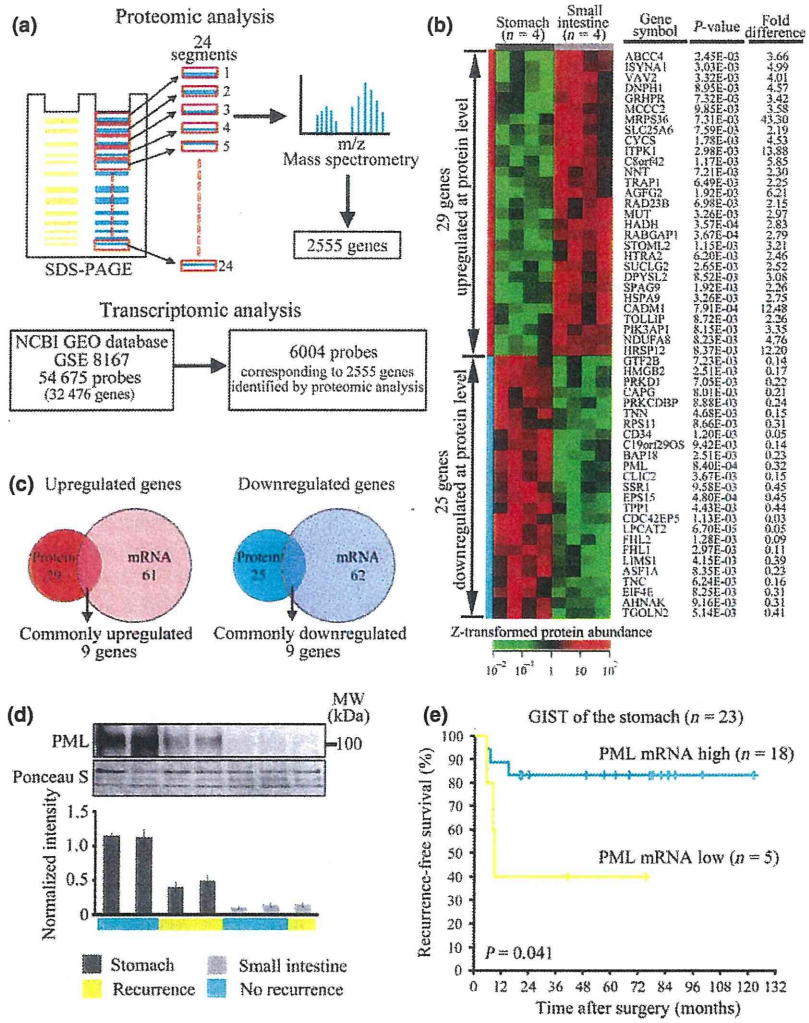

Fig. 1. Integrated proteomic and transcriptomic analysis shows promyelocytic leukemia (PML) downregulation in gastrointestinal stromal tumors (GIST) of the small intestine (I-GIST), and its potential as a prognostic biomarker. Workflow of the proteomic and transcriptomic analysis (a). Heatmap of the genes differentially expressed at the protein level (b). Venn diagrams showing the numbers of commonly upregulated and downregulated genes at both the protein and mRNA levels (c). Western blotting shows the differences in PML expression between the samples used for proteomic analysis (d). Kaplan–Meier analysis of recurrence-free survival according to the expression of PML mRNA in S-GIST of GSE8167 (e).

defined as positively stained if their nuclear staining intensity with the anti-PML antibody was equal to or higher than that of vascular endothelial cells used as an internal positive control in the same section. The examined cases were divided into negative (positive nuclear staining in <10% of tumor cells), focally positive (in ≥10% or more but <50%) and diffusely positive (in ≥50%), as previously reported.[29] In most cases, the difference was quite obvious and the two reviewers concurred as to the results.

Statistical analysis. Fisher's exact test was used to evaluate the correlations between PML expression status and clinicopathological characteristics. The correlation coefficients between these variables were evaluated using Spearman rank correlation analysis. The RFS was calculated from the date of initial surgery to that of first recurrence, censoring patients alive at the time of data collection and those who died without recurrence on the date of death. The RFS rate was estimated using the Kaplan–Meier method.[30] Univariate survival analyses were performed using the log-rank test. The Cox proportional hazards model was applied to the multivariate survival analysis.[31] The variables with a univariate $P < 0.05$ were entered into the model. Differences at $P < 0.05$ were regarded as statistically significant. SPSS version 11.5 (SPSS, Chicago, IL, USA) was used for all of the statistical analyses.

Results

Genes showing differences in protein expression specific to the tumor site. Using label-free proteomic analysis, we identified and quantified 26 832 unique peptides corresponding to 2550 non-redundant proteins from 8 GIST (Suppl. Tables S4 and S5). Unsupervised analysis showed that the samples were grouped according to the tumor site and whether or not the tumor recurred (Suppl. Fig. S1). These observations suggested that the overall protein expression profiles reflected the difference in the tumor site and malignant potential. Among the 2550 genes, 29 were significantly upregulated and 25 were

Table 2. Upregulated or downregulated genes in GIST of the small intestine at both protein and mRNA level

Gene symbol†	Gene description	Locus	Protein			mRNA			
			Accession number‡	*P*-value§	Fold difference¶	Probe set ID††	Accession number‡‡	*P*-value§§	Fold difference§
Upregulated genes									
ABCC4	Multidrug resistance-associated protein 4	13q32	O15439	2.45E-03	3.66	203196_at	AI948503	1.98E-03	3.27
						1554918_a_at	BC041560	6.27E-03	2.95
						1555039_a_at	AY133679	1.53E-03	2.69
AGFG2	Arf-GAP domain and FG repeats-containing protein 2	7q22.1	O95081	1.92E-03	6.21	206821_x_at	NM_006076	2.29E-04	2.87
						217450_at	AF053356	2.53E-05	2.91
						222126_at	AI247494	8.07E-04	5.04
						222362_at	H07885	6.96E-04	4.28
						1554618_at	BC009393	4.35E-04	3.20
ISYNA1	Inositol-3-phosphate synthase 1		O43598	8.95E-03	4.57	222240_s_at	AL137749	8.27E-03	2.11
CYCS	Cytochrome c	7p15.3	P99999	1.78E-03	4.53	208905_at	BC005299	2.46E-05	2.22
						229415_at	BF593856	5.12E-04	2.44
						244546_at	AI760495	8.34E-04	2.22
ITPK1	Inositol-tetrakisphosphate 1-kinase	14q31	Q13572	2.98E-03	13.88	210197_at	BC003622	4.91E-04	2.22
						210740_s_at	AF279372	1.59E-08	15.38
CADM1	Cell adhesion molecule 1	11q23.2	Q9BY67	7.91E-04	12.48	209030_s_at	NM_014333	1.24E-05	20.96
						209031_at	AL519710	2.95E-05	25.62
						209032_s_at	AF132811	1.70E-06	9.96
						244345_at	AI627453	2.90E-05	2.17
DNPH1	2′-deoxynucleoside 5′-phosphate N-hydrolase 1	6p21.1	O43598	8.95E-03	4.57	204238_s_at	NM_006443	1.93E-03	2.69
						39817_s_at	AF040105	2.14E-04	2.06
C8orf42	Chromosome 8 open reading frame 42	8p23.3	Q86YL5	1.17E-03	5.85	226778_at	AI632224	7.35E-04	2.75
						230903_s_at	H11634	2.22E-05	3.40
PIK3AP1	Phosphoinositide 3-kinase adapter protein 1	10q24.1	Q6ZUJ8	8.15E-03	3.35	226459_at	AW575754	3.15E-05	6.55
						1554508_at	BC029917	5.64E-07	4.51
Downregulated genes									
AHNAK	Neuroblast differentiation-associated protein AHNAK	11q12.2	Q09666	9.16E-03	0.31	211986_at	BG287862	6.36E-03	0.45
PML	Promyelocytic leukemia	15q22	P29590	8.40E-04	0.32	235508_at	AW291023	1.88E-06	0.42
CLIC2	Chloride intracellular channel protein 2	Xq28	O15247	3.67E-03	0.15	213415_at	AI768628	1.02E-06	0.18
CD34	CD34 molecule	1q32	P28906	1.20E-03	0.05	209543_s_at	M81104	8.83E-08	0.07
LPCAT2	Lysophosphatidylcholine acyltransferase 2	16q12.2	Q7L5N7	6.70E-05	0.05	227889_at	AI765437	1.30E-06	0.06
						222833_at	AU154202	1.01E-05	0.24
						239598_s_at	AA789296	7.19E-03	0.34
FHL2	Four and a half LIM domains protein 2	2q12.2	Q14192	1.28E-03	0.09	202949_s_at	NM_001450	1.36E-06	0.15
EPS15	Epidermal growth factor receptor substrate 15	1p32	P42566	4.80E-04	0.45	217887_s_at	NM_001981	3.48E-07	0.45
						217886_at	BF213575	2.90E-07	0.47
PRKCDBP	Protein kinase C delta-binding protein	11p15.4	Q969G5	8.88E-03	0.24	213010_at	AI088622	1.41E-06	0.16
CDC42EP5	Cdc42 effector protein 5	19q13.42	Q6NZY7	1.13E-03	0.03	227850_x_at	AW084544	7.84E-08	0.16

†Gene symbols were derived from UniGene. ‡Accession numbers of proteins were derived from Swiss-Prot and NCBI nonredundant databases. §*P*-values were calculated by *t*-test. ¶Fold differences were calculated by dividing the mean normalized expression value of GIST of the small intestine samples by that of GIST of the stomach samples. ††Affymetrix Human Genome U133 Plus 2.0 Array probe set ID. ‡‡Accession numbers of genes were derived from GenBank database. §§*P*-values were calculated by *t*-test and corrected by Benjamini–Hochberg false discovery rate. GIST, gastrointestinal stromal tumors.

downregulated at the protein level in I-GIST ($P < 0.01$; fold difference ≥2.0, Fig. 1b and Suppl. Table S6).

Genes showing differences in mRNA expression specific to the tumor site. From the GSE8167 dataset, we extracted 6004 probes corresponding to the genes observed in the proteomic analysis (Suppl. Table S7). Similarly to the protein expression profiles, unsupervised analysis showed that the overall features of mRNA expression reflected the difference in the tumor site (Suppl. Fig. S2). Among the 2555 genes corresponding to the 6004 probes, 65 genes (115 probes) were significantly upregulated and 67 genes (108 probes) were downregulated at the mRNA level in I-GIST ($P < 0.01$; fold difference ≥2.0, Suppl. Fig. S3 and Suppl. Table S8).

Integrated proteomic and transcriptomic analysis. We observed the 54 and 132 genes that were differentially expressed at the protein and mRNA levels. A total of 9 genes

were commonly upregulated and 9 were commonly downregulated in I-GIST at both the protein and mRNA level (Suppl. Fig. 1c and Table 2). CD34 protein and mRNA had been previously reported to be downregulated in I-GIST,[10,15] and our present study identified CD34 as a commonly downregulated gene in I-GIST (Table 2). Therefore, the other genes that were identified in our study may also be potentially related to the tumor site, and probably contribute to the malignant behavior of I-GIST.

The promyelocytic leukemia gene (*PML*) was included among the 9 genes that were commonly downregulated (Table 2 and Fig. S4). PML protein was originally identified as a fusion partner of the retinoic acid receptor-α (RARα) in the transforming protein (PML-RARα) found in acute promyelocytic leukemias.[32] PML functions as a tumor suppressor that controls apoptosis, protein synthesis, the cell cycle, cellular proliferation and genomic stability.[33] Loss of PML has been reported in breast cancer, gastric cancer and small cell lung cancer, but not in GIST.[34] In addition, *PML* is located on chromosome 15q, which is frequently lost in I-GIST,[17] suggesting that the decreased level of PML might reflect genomic alteration in I-GIST. With these notions, we further explored PML expression in GIST and its clinical utility.

Promyelocytic leukemia as a potential novel prognostic marker in gastrointestinal stromal tumors. Western blotting of the samples used for proteomic analysis revealed that PML protein was downregulated in I-GIST, being consistent with the result of the proteomic analysis. Moreover, we found that PML protein was also downregulated in the tumor of S-GIST obtained from patients who developed postoperative recurrence (Fig. 1d). We then analyzed the expression of PML mRNA in 23 cases of S-GIST using the transcriptome dataset. The appropriate cut-off value for the prediction of postoperative recurrence was set at −0.094 with a sensitivity of 88.2% and a specificity of 50.0% by the receiver operating characteristic curve (Suppl. Fig. S5). We divided 23 cases into two groups showing high (n = 18) and low (n = 5) expression by this value. Kaplan–Meier analysis demonstrated

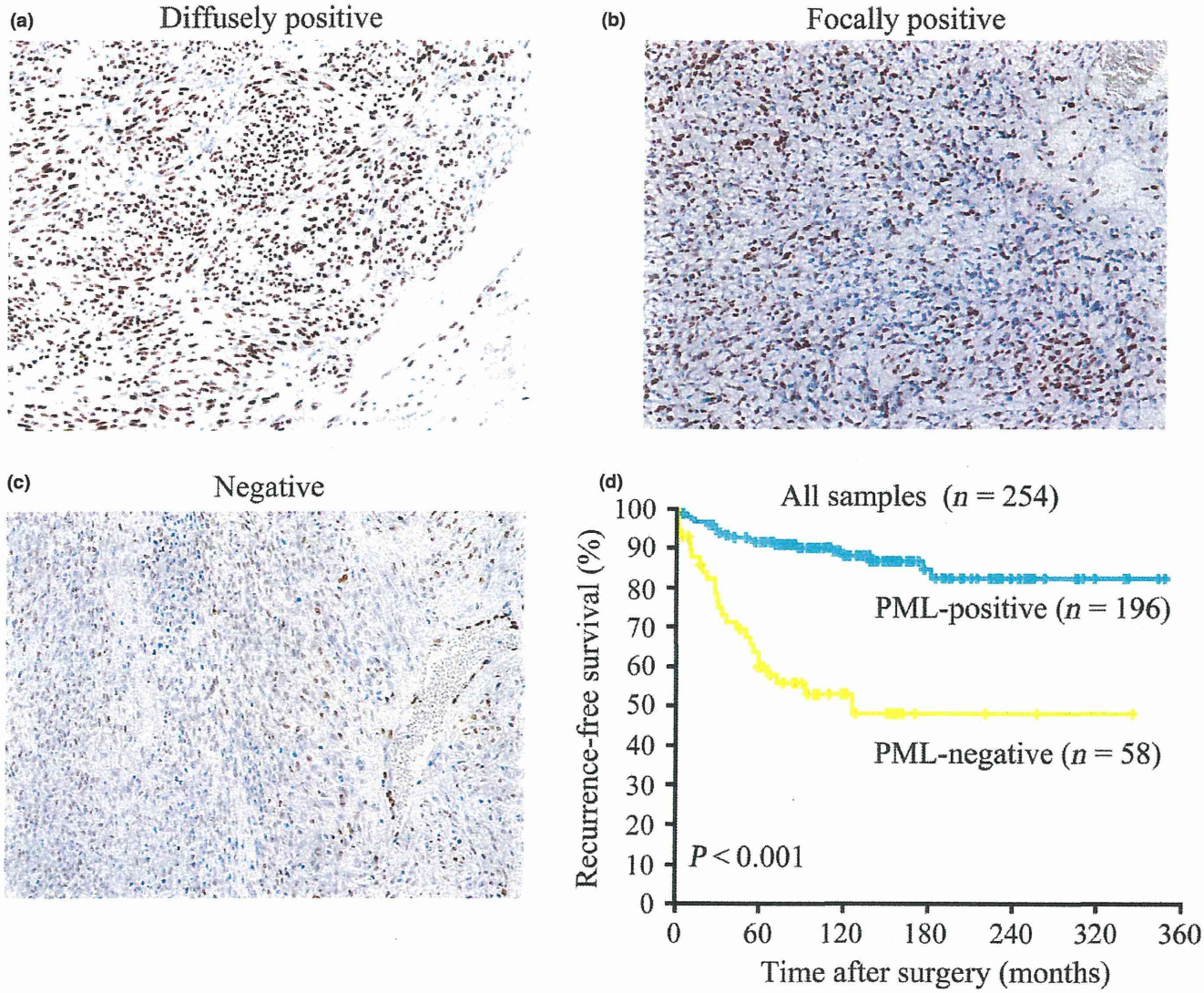

Fig. 2. Immunohistochemical validation study of promyelocytic leukemia (PML) expression. PML is diffusely positive in gastrointestinal stromal tumors (GIST) of the stomach (S-GIST) (a), whereas it is focally positive in S-GIST with recurrence (b), and it is not expressed in GIST of the small intestine (c). Kaplan–Meier analysis of recurrence-free survival according to PML expression in samples from multiple clinical facilities (d).

that the RFS period of patients with low expression of PML mRNA was significantly shorter than that of patients with high expression ($P = 0.041$) (Fig. 1e). PML was downregulated not only in I-GIST but also in S-GIST showing malignant behavior, and has the potential to be a novel prognostic marker in GIST.

Immunohistochemical validation study using gastrointestinal stromal tumor cases from multiple clinical facilities. We validated the correlation of PML expression with the tumor site and patients' outcome using immunohistochemistry in 254 additional samples from the National Cancer Center Hospital (156 cases) and Niigata University Hospital (98 cases). PML immunostaining showed a nuclear speckled pattern or a diffuse nucleoplasmic pattern (Fig. 2a–c). Vascular endothelial cells were strongly positive for PML expression, as described in a previous report.[34] Among the 254 cases, 196 cases (77.2%) showed diffusely positive staining and were classified as PML-positive. The remaining 46 cases (18.1%) showing focal positivity and 12 cases (4.7%) that were negative were classified as PML-negative. Thirty-six of 211 cases with S-GIST (17.0%), 12 of 22 cases with I-GIST (54.5%) and 10 of 21 cases arising in other organs (47.6%) showed PML-negative, the differences being statistically significant ($P < 0.001$). Expression of PML was also correlated with tumor size ($P < 0.001$), mitosis ($P < 0.001$) and NIH consensus criteria ($P < 0.001$) as well as the tumor site (Table 3). Kaplan–Meier survival analysis showed that the 5-year RFS rate was significantly lower for PML-negative than for PML-positive cases (60.1% *vs* 91.7%; $P < 0.001$) (Table 3 and Fig. 2d). Tumor site, histologic subtype, tumor size, mitosis and NIH consensus criteria were also significantly correlated with RFS in the univariate analysis. The correlation coefficient between NIH consensus criteria and tumor size was 0.78, and that between NIH consensus criteria and mitosis was 0.71 (Suppl. Table S9). They were especially high among those between other variables. Therefore, tumor size and mitosis were excluded from the variables entered into the Cox proportional hazards model to avoid multicollinearity. As a result, PML negativity was an independent unfavorable prognostic factor (hazard ratio [HR] = 2.739; $P = 0.001$) in addition to an indicator of a

Table 3. Correlations between clinicopathological characteristics and immunohistochemical expression of PML and survival analysis in the 254 GIST patients of the NCCH and Niigata University Hospital

Variable	Number of patients ($N = 254$)	PML expression		*P*-value	Univariate analysis		Multivariate analysis‡		
		Positive ($N = 196$)	Negative ($N = 58$)		5-year RFS rate (%)†	*P*-value	Hazard ratio	95% CI	*P*-value
Age									
<60	103	75	28	0.173	78.5	0.184	Not included		
≥60	151	121	30		88.8				
Gender									
Female	130	95	35	0.112	88.8	0.199	Not included		
Male	124	101	23		80.2				
Tumor site									
Stomach	211	175	36	<0.001	88.7	<0.001	1.000		
Small intestine	22	10	12		59.1		2.130	0.985–4.609	0.055
Other	21	11	10		71.1		1.531	0.686–3.418	0.298
Histologic subtype									
Spindle	198	157	41	0.350	90.7	<0.001	1.000		
Epithelioid	17	13	4		70.6		1.849	0.740–4.618	0.188
Mixed	37	25	12		57.0		1.699	0.859–3.359	0.128
Unknown§	2	1	1		—		—	—	—
Size (cm)									
≤5	154	132	22	<0.001	93.3	<0.001	Not included		
5.1–10.0	75	50	25		75.7				
>10	25	14	11		58.8				
Mitosis (/50 HPF)									
≤5	185	155	30	<0.001	95.0	<0.001	Not included		
6–10	43	27	16		73.2				
>10	26	14	12		28.2				
Risk classification¶									
Very low or low	122	107	15	<0.001	96.6	<0.001	1.000		
Intermediate	71	56	15		91.4		2.808	0.937–8.411	0.065
High	61	33	28		52.5		13.121	4.877–35.301	<0.001
PML expression									
Positive	196	—	—	—	91.7	<0.001	1.000		
Negative	58	—	—		60.1		2.739	1.498–5.006	0.001

†Five-year RFS rates were estimated by the Kaplan–Meier method. ‡In addition to PML expression status, covariates of tumor site, histologic subtype and recurrence risk classification were included in the multivariate analysis. §Two cases of unknown histologic subtype were not included in the survival analysis. ¶Recurrence risk was classified according to the NIH consensus criteria. CI, confidence interval; GIST, gastrointestinal stromal tumors; HPF, high power fields; PML, promyelocytic leukemia; RFS, recurrence-free survival.

high-risk of recurrence according to the NIH consensus criteria (HR = 13.121; $P < 0.001$).

We then examined the prognostic value of PML expression in cases stratified according to the tumor site or NIH consensus criteria (Fig. 3). In the S-GIST group, the 5-year RFS rate was 61.2% for PML-negative cases and 94.2% for PML-positive cases ($P < 0.001$; Fig. 3a). In contrast, in the I-GIST and other anatomical tumor site group, the difference between PML-positive and negative cases was not statistically significant (Fig. 3b,c). With regard to the NIH consensus criteria, the RFS rate was significantly lower in PML-negative than in PML-positive cases within each risk group (Fig. 3d–f).

Discussion

The prognosis of GIST patients differs according to the tumor site; I-GIST show more aggressive behavior than S-GIST.[11] Genome-wide global studies have revealed differences in *KIT* or *PDGFRA* mutations, gene expressions and chromosomal aberrations between I-GIST and S-GIST.[13–20] These observations suggest that further exploration of these molecular aberrations associated with the tumor site would yield clues to understanding the molecular background of the malignancy in GIST, thus widening the clinical options available to GIST patients.

This is the first report of the integrated proteomic and transcriptomic analysis of GIST aimed at exploring the molecular differences associated with the tumor site and prognostic biomarkers. The proteome is the functional translation of the genome, by which tumor cell phenotypes are directly regulated. Therefore, the proteomic analysis has considerable potential for discovery of biomarkers based on the molecular backgrounds of tumor malignancy. Proteomics can identify many proteins showing differential expressions. Thus, selection and validation of biomarker candidates is critical in the biomarker study. Recently, transcriptome data for well characterized clinical materials became publically available, and meta-analysis has been performed to assess the clinical utilities of biomarker candidates at the mRNA level. This is in contrast to proteome data, as few such data for clinical materials are publicly available. For proteins whose expression levels show concordance with those of the corresponding mRNA, it is possible to verify their utility as biomarkers using western blotting and immunohistochemistry at the protein level, or RT-PCR and meta-analysis of public transcriptomic data at the mRNA level. Against this background, we challenged the biomarker discovery at both the protein and mRNA levels.

We identified *PML* as a commonly downregulated gene in I-GIST at both the protein and mRNA levels. PML regulates oncogenic pathways such as the cell cycle, apoptosis and angiogenesis through interaction with pRB, p53, MDM2, PTEN, mTOR and HIF-1α.[33] *PML* is one of the tumor suppressor genes, and its loss leads to alteration of these pathways. These oncogenic pathways reported to play a major role in the molecular biology of GIST through the constitutive activation of KIT or PDGFRA signaling (Suppl. Fig. S6). GIST with high-risk of recurrence show significant changes in genes that regulate the cell cycle.[35] *TP53* mutations, p53 overexpression and *MDM2* amplification are correlated with poor outcome in GIST patients.[36,37] The PI3K-mTOR signaling pathway is one of the most important for growth of GIST cells.[38] HIF-1α plays an important role in GIST angiogenesis, and high expression is correlated with recurrence and metastasis.[39] Therefore, downregulation of PML might contribute to the malignant behavior of I-GIST.

We validated the association of PML expression with the tumor site and confirmed its prognostic utility in additional cases of GIST from multiple clinical facilities using immunohistochemistry. Downregulation of PML expression was significantly associated with not only I-GIST, but also a larger tumor size, higher mitotic count and higher risk of recurrence (Table 3). These results are consistent with the abovementioned tumor suppressive function of PML because these findings reflect higher cell proliferation based on dysregulation of the cell cycle or apoptosis. Survival analysis showed that PML expression was significantly correlated with the RFS period; identical results were obtained in cases stratified according to their institutions of origin (Suppl. Fig. S7 and S8; Suppl. Tables S10 and S11). The stratified survival analysis showed that PML expression was significantly correlated with the RFS period in the S-GIST group, but not in the I-GIST and other sites group. Therefore, PML could be applied as a prognosticator to patients with S-GIST. I-GIST and GIST arising from other sites were minorities in GIST, and the number of cases examined was small. Further analyses are needed to elucidate the benefit of PML evaluation in these types of GIST.

Recent studies indicated that adjuvant imatinib administration was relevant for NIH high-risk patients, but the evidence on intermediate-risk patients is insufficient.[9] In our analysis, prognostic significance of PML expression was independent from that of NIH consensus criteria. PML expression could clearly distinguish between better and worse prognosis of patients within the NIH intermediate-risk group, and the 5-year RFS rate of the PML-negative cases was 71.8%. Thus, PML evaluation to select patients suitable for adjuvant therapy with imatinib may be applicable to the intermediate-risk group. However, the difference of RFS according to PML expression in the NIH very low or low-risk group was statistically significant, but PML-negative cases had relatively good prognosis; the 5-year survival rate was 86.2%. Therefore, adjuvant imatinib administration is considered as over-treatment for patients in the NIH very low or low-risk group regardless of PML expression. However, further prospective analyses are necessary to clarify the utility of PML evaluation for an optimization of the adjuvant therapy.

Our study was limited in that we did not examine the molecular functions of PML *in vivo* and *in vitro*. Recently, inhibition of the PML degradation pathway using a proteasome inhibitor has been show to preserve its expression, thus making it an attractive approach for anti-cancer therapy.[40] We examined the effects of a proteasome inhibitor on PML protein expression in GIST cells (GIST-T1), and found that the inhibitor did not preserve PML protein expression, probably because it is controlled predominantly at the mRNA level and not at the protein degradation level in GIST cells (Suppl. Fig. S9). Further analysis of the functional significance of PML will lead to a more detailed understanding of the disease mechanisms of GIST, thus helping to reveal novel therapeutic modalities.

In conclusion, through integrated proteomic and transcriptomic analysis, we demonstrated differential expressions of 18 genes associated with the tumor site. Among them, we identified *PML*, a tumor suppressor gene, as a commonly downregulated gene at both the protein and mRNA levels in I-GIST. Using additional cases from multiple clinical facilities, we successfully validated the association of PML downregulation

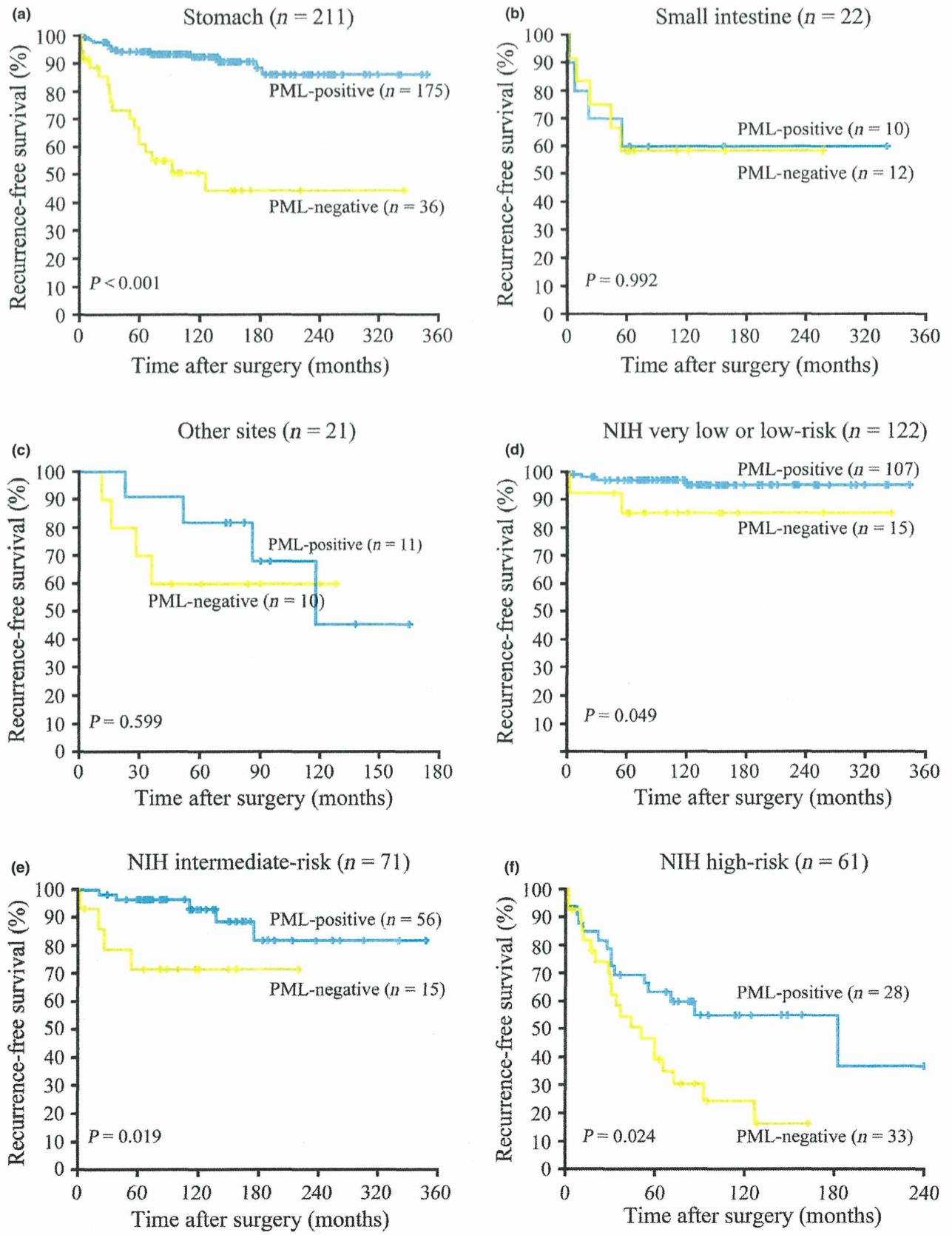

Fig. 3. The stratified Kaplan–Meier analysis of recurrence-free survival. The cases were stratified according to the tumor site (a–c), and stratified according to recurrence risk classification of the NIH consensus criteria (d–f).

with I-GIST and a shorter RFS period. Prognostication using PML expression may help to optimize the treatment strategy for GIST patients.

Disclosure Statement

The authors have no conflict of interest to declare.

References

1 Rubin BP, Heinrich MC, Corless CL. Gastrointestinal stromal tumour. *Lancet* 2007; **369**: 1731–41.
2 Hirota S, Isozaki K, Moriyama Y *et al.* Gain-of-function mutations of c-kit in human gastrointestinal stromal tumors. *Science* 1998; **279**: 577–80.
3 Hirota S, Ohashi A, Nishida T *et al.* Gain-of-function mutations of platelet-derived growth factor receptor alpha gene in gastrointestinal stromal tumors. *Gastroenterology* 2003; **125**: 660–7.
4 Heinrich MC, Corless CL, Duensing A *et al.* PDGFRA activating mutations in gastrointestinal stromal tumors. *Science* 2003; **299**: 708–10.
5 Corless CL, Barnett CM, Heinrich MC. Gastrointestinal stromal tumours: origin and molecular oncology. *Nat Rev Cancer* 2011; **11**: 865–78.
6 Dematteo RP, Ballman KV, Antonescu CR *et al.* Adjuvant imatinib mesylate after resection of localised, primary gastrointestinal stromal tumour: a randomised, double-blind, placebo-controlled trial. *Lancet* 2009; **373**: 1097–104.
7 Kanda T, Nishida T, Wada N *et al.* Adjuvant therapy with imatinib mesylate after resection of primary high-risk gastrointestinal stromal tumors in Japanese patients. *Int J Clin Oncol* 2013; **18**: 38–45.
8 Joensuu H, Eriksson M, Sundby Hall K *et al.* One vs three years of adjuvant imatinib for operable gastrointestinal stromal tumor: a randomized trial. *JAMA* 2012; **307**: 1265–72.
9 Joensuu H. Adjuvant treatment of GIST: patient selection and treatment strategies. *Nat Rev Clin Oncol* 2012; **9**: 351–8.
10 Miettinen M, Lasota J. Gastrointestinal stromal tumors – definition, clinical, histological, immunohistochemical, and molecular genetic features and differential diagnosis. *Virchows Arch* 2001; **438**: 1–12.
11 Emory TS, Sobin LH, Lukes L, Lee DH, O'Leary TJ. Prognosis of gastrointestinal smooth-muscle (stromal) tumors: dependence on anatomic site. *Am J Surg Pathol* 1999; **23**: 82–7.
12 Joensuu H. Risk stratification of patients diagnosed with gastrointestinal stromal tumor. *Hum Pathol* 2008; **39**: 1411–9.
13 Antonescu CR, Sommer G, Sarran L *et al.* Association of KIT exon 9 mutations with nongastric primary site and aggressive behavior: KIT mutation analysis and clinical correlates of 120 gastrointestinal stromal tumors. *Clin Cancer Res* 2003; **9**: 3329–37.
14 Haller F, Happel N, Schulten H-J *et al.* Site-dependent differential KIT and PDGFRA expression in gastric and intestinal gastrointestinal stromal tumors. *Mod Pathol* 2007; **20**: 1103–11.
15 Antonescu CR, Viale A, Sarran L *et al.* Gene expression in gastrointestinal stromal tumors is distinguished by KIT genotype and anatomic site. *Clin Cancer Res* 2004; **10**: 3282–90.
16 Chen Y, Tzeng C-C, Liou C-P, Chang M-Y, Li C-F, Lin C-N. Biological significance of chromosomal imbalance aberrations in gastrointestinal stromal tumors. *J Biomed Sci* 2004; **11**: 65–71.
17 Gunawan B, Schulten H-J, von Heydebreck A *et al.* Site-independent prognostic value of chromosome 9q loss in primary gastrointestinal stromal tumours. *J Pathol* 2004; **202**: 421–9.
18 Nishitani A, Hirota S, Nishida T *et al.* Differential expression of connexin 43 in gastrointestinal stromal tumours of gastric and small intestinal origin. *J Pathol* 2005; **206**: 377–82.
19 Wozniak A, Sciot R, Guillou L *et al.* Array CGH analysis in primary gastrointestinal stromal tumors: cytogenetic profile correlates with anatomic site and tumor aggressiveness, irrespective of mutational status. *Genes Chromosom Cancer* 2007; **46**: 261–76.
20 Yamaguchi U, Nakayama R, Honda K *et al.* Distinct gene expression-defined classes of gastrointestinal stromal tumor. *J Clin Oncol* 2008; **26**: 4100–8.
21 Schirle M, Heurtier M-A, Kuster B. Profiling core proteomes of human cell lines by one-dimensional PAGE and liquid chromatography-tandem mass spectrometry. *Mol Cell Proteomics* 2003; **2**: 1297–305.
22 Jafari M, Primo V, Smejkal GB, Moskovets EV, Kuo WP, Ivanov AR. Comparison of in-gel protein separation techniques commonly used for fractionation in mass spectrometry-based proteomic profiling. *Electrophoresis* 2012; **33**: 2516–26.
23 Li Z, Adams RM, Chourey K, Hurst GB, Hettich RL, Pan C. Systematic comparison of label-free, metabolic labeling, and isobaric chemical labeling for quantitative proteomics on LTQ Orbitrap Velos. *J Proteome Res* 2012; **11**: 1582–90.
24 Suehara Y, Kondo T, Seki K *et al.* Pfetin as a prognostic biomarker of gastrointestinal stromal tumors revealed by proteomics. *Clin Cancer Res* 2008; **14**: 1707–17.
25 Bosman FT, Carneiro F, Hruban RH, Theise ND. *WHO Classification of Tumours of the Digestive System*, 4th edn. Geneva: IARC Press, 2010.
26 Fletcher CD, Berman JJ, Corless C *et al.* Diagnosis of gastrointestinal stromal tumors: a consensus approach. *Hum Pathol* 2002; **33**: 459–65.
27 Kondo T, Hirohashi S. Application of highly sensitive fluorescent dyes (CyDye DIGE Fluor saturation dyes) to laser microdissection and two-dimensional difference gel electrophoresis (2D-DIGE) for cancer proteomics. *Nat Protoc* 2006; **1**: 2940–56.
28 Irizarry RA, Hobbs B, Collin F *et al.* Exploration, normalization, and summaries of high density oligonucleotide array probe level data. *Biostatistics* 2003; **4**: 249–64.
29 Lee HE, Jee CD, Kim MA *et al.* Loss of promyelocytic leukemia protein in human gastric cancers. *Cancer Lett* 2007; **247**: 103–9.
30 Kaplan EL, Meier P. Nonparametric estimation from incomplete observations. *J Am Stat Assoc* 1958; **53**: 457–81.
31 Cox D. Regression model and life tables. *J Royal Stat Soc* 1972; **B34**: 187–220.
32 Melnick A, Licht JD. Deconstructing a disease: RARalpha, its fusion partners, and their roles in the pathogenesis of acute promyelocytic leukemia. *Blood* 1999; **93**: 3167–215.
33 Salomoni P, Ferguson BJ, Wyllie AH, Rich T. New insights into the role of PML in tumour suppression. *Cell Res* 2008; **18**: 622–40.
34 Gurrieri C, Capodieci P, Bernardi R *et al.* Loss of the tumor suppressor PML in human cancers of multiple histologic origins. *J Natl Cancer Inst* 2004; **96**: 269–79.
35 Haller F, Gunawan B, von Heydebreck A *et al.* Prognostic role of E2F1 and members of the CDKN2A network in gastrointestinal stromal tumors. *Clin Cancer Res* 2005; **11**: 6589–97.
36 Zong L, Chen P, Jiang J, Wang L, Li QG. Predictive value of p53 expression in the risk of malignant gastrointestinal stromal tumors: evidence from 19 studies. *Exp Ther Med* 2012; **3**: 87–92.
37 Tornillo L, Duchini G, Carafa V *et al.* Patterns of gene amplification in gastrointestinal stromal tumors (GIST). *Lab Invest* 2005; **85**: 921–31.
38 Bauer S, Duensing A, Demetri GD, Fletcher JA. KIT oncogenic signaling mechanisms in imatinib-resistant gastrointestinal stromal tumor: PI3-kinase /AKT is a crucial survival pathway. *Oncogene* 2007; **26**: 7560–8.
39 Chen W-T, Huang C-J, Wu M-T, Yang S-F, Su Y-C, Chai C-Y. Hypoxia-inducible factor-1alpha is associated with risk of aggressive behavior and tumor angiogenesis in gastrointestinal stromal tumor. *Jpn J Clin Oncol* 2005; **35**: 207–13.
40 Chen R-H, Lee Y-R, Yuan W-C. The role of PML ubiquitination in human malignancies. *J Biomed Sci* 2012; **19**: 81.

Supporting Information

Additional supporting information may be found in the online version of this article:

Fig. S1. Unsupervised analysis according to the protein expression of 2555 genes.

Fig. S2. Unsupervised analysis according to the mRNA expression of 2555 genes.

Fig. S3. Heat-map of the 132 genes (223 probes) showing differences in mRNA expression between S-GIST and I-GIST.

Fig. S4. The difference in promyelocytic leukemia (PML) expression between S-GIST and I-GIST revealed by proteomic and transcriptomic analysis.

Fig. S5. Receiver operating characteristic curve of promyelocytic leukemia (PML) mRNA expression as a discriminator of recurrence status in the S-GIST group.

Fig. S6. Schema of the interaction between promyelocytic leukemia (PML) and gastrointestinal stromal tumors (GIST) oncogenic pathways lying downstream of KIT or PDGFRA.

Fig. S7. Immunohistochemical validation study of promyelocytic leukemia (PML) expression in the 156 gastrointestinal stromal tumors (GIST) cases from the National Cancer Center Hospital.

Fig. S8. Immunohistochemical validation study of promyelocytic leukemia (PML) expression in the 98 gastrointestinal stromal tumors (GIST) cases from Niigata University Hospital.

Fig. S9. Effects of a proteasome inhibitor, bortezonib, on promyelocytic leukemia (PML) expression in GIST-T1 cells.

Table S1. Clinicopathological characteristics of the 156 gastrointestinal stromal tumors (GIST) cases from the National Cancer Center Hospital.

Table S2. Clinicopathological characteristics of the 98 gastrointestinal stromal tumors (GIST) cases from Niigata University Hospital.

Table S3. Clinicopathological characteristics of the samples used in the transcriptomic analysis.

Table S4. Details of 2555 proteins analyzed by Progenesis LC-MS.

Table S5. Details of peptides assigned to 2555 proteins.

Table S6. Genes differentially expressed at the protein level in I-GIST.

Table S7. Details of 6004 probes corresponding to 2555 genes identified in the proteomic analysis.

Table S8. Genes differentially expressed at the mRNA level in I-GIST.

Table S9. The correlation coefficients between the clinicopathological characteristics.

Table S10. Correlations between clinicopathological characteristics and immunohistochemical expression of promyelocytic leukemia (PML) and survival analysis in gastrointestinal stromal tumors (GIST) cases from the National Cancer Center Hospital.

Table S11. Correlations between clinicopathological characteristics and immunohistochemical expression of promyelocytic leukemia (PML) and survival analysis in gastrointestinal stromal tumors (GIST) cases from Niigata University Hospital.

Doc. S1. Supporting materials and methods.

Journal of proteome research

Article

pubs.acs.org/jpr

Proteomics Identified Overexpression of SET Oncogene Product and Possible Therapeutic Utility of Protein Phosphatase 2A in Alveolar Soft Part Sarcoma

Daisuke Kubota,[†,‡] Akihiko Yoshida,[§] Akira Kawai,[‡] and Tadashi Kondo*[,†]

[†]Division of Pharmacoproteomics, National Cancer Center Research Institute, Tsukiji 5-1-1, Chuo-ku, Tokyo 104-0045, Japan

[‡]Division of Musculoskeletal Oncology and [§]Pathology and Clinical Laboratory Division, National Cancer Center Hospital, Tsukiji 5-1-1, Chuo-ku, Tokyo 104-0045, Japan

Supporting Information

ABSTRACT: Alveolar soft part sarcoma (ASPS) is an exceedingly rare sarcoma refractory to standard chemotherapy. Although several molecular targeting drugs have been applied for ASPS, their clinical significance has not yet been established, and novel therapeutic strategies have long been required. The aim of this study was to identify proteins aberrantly regulated in ASPS and to clarify their clinical significance. Protein expression profiling of tumor and nontumor tissues from 12 ASPS patients was performed by 2-D difference gel electrophoresis and mass spectrometry. We found that the expression of 145 proteins differed significantly. Among them, further investigation was focused on the SET protein, which has multifunctional roles in cancers. Immunohistochemistry confirmed overexpression of SET in all 15 ASPS cases examined. Gene silencing of SET significantly decreased cell proliferation, invasion, and migration against a background of induced apoptosis. SET is known to be an inhibitor of phosphatase 2A (PP2A), which functions as a tumor suppressor by inhibiting the signal transduction pathway and inducing apoptosis. We found that a PP2A activator, FYN720, decreased cell proliferation through apoptosis. Together, our findings may suggest the possible contribution of SET to the tumor progression and the utility of FYN720 for treatment of ASPS.

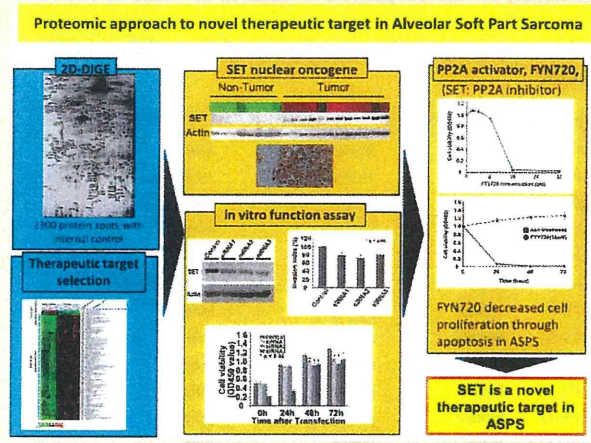

1. INTRODUCTION

Alveolar soft part sarcoma (ASPS) is an exceedingly rare sarcoma that accounts for fewer than 1% of all soft tissue sarcomas.[1] While patients can often achieve prolonged survival after surgery, even if metastases are present, most eventually succumb to the disease as a result of late metastasis. Both standard cytotoxic chemotherapy and radiation therapy have no significant survival advantage, and an effective molecular targeting drug has long been sought. ASPS is characterized by the presence of chromosomal rearrangement at 17q25 and Xp11.2, engendering a fusion gene, ASPSCR1-TFE3, which is a superactivated chimeric transcription factor.[2] Recent global gene expression profiling has identified an array of genes that are possibly regulated by the ASPSCR1-TFE3 fusion gene, and these genes include potentially therapeutic targets.[3−5] One of the critical genes induced by ASPSCR1-TFE3 and playing a role in disease progression is the angiogenesis-promoting oncogene, MET.[3] This molecular background has led to the introduction of antiangiogenic agents such as INF-alpha,[6−8] bevacizumab,[9,10] sunitinib,[11−13] and cediranib for ASPS. The clinical efficacies of these novel molecular targeting agents will be validated in large-scale clinical studies.

In the present investigation, in order to clarify the molecular pathogenesis of ASPS and identify proteins that might have clinical utility, we performed a proteomic study of ASPS. While proteomics has been applied to a variety of cancers to identify biomarkers and therapeutic targets,[14] no proteomics study of ASPS has been reported, except for one in which only one formalin-fixed and paraffin-embedded ASPS tissue was examined using a shotgun approach.[15] We identified proteins that were uniquely expressed in the tumor tissues, and further focused on one oncogene product, suppressor of variegation, enhancer of zeste, and trithorax (SET), which was originally reported as a chimeric gene in acute myelocytic leukemia.[16] We confirmed the overexpression of SET in ASPS by Western blotting and immunohistochemistry and verified the functional significance of SET by a gene-silencing assay. SET is a specific inhibitor of a

Received: September 12, 2013

   dx.doi.org/10.1021/pr400929h | J. Proteome Res. XXXX, XXX, XXX−XXX

tumor suppressor, phosphatase 2A (PP2A),[17] which is deregulated in several malignancies.[18] We revealed that a PP2A activator, FYN720, exerted antitumor effects on ASPS cells. Our study reveals novel aspects of SET in ASPS and suggests possible therapeutic application of a PP2A inhibitor for this malignancy.

2. MATERIALS AND METHODS

2.1. Patients, Cell Line, and Protein Samples

This study included all 15 cases of ASPS that had been diagnosed and treated at the National Cancer Center Hospital between 1996 and 2010. Metastasis was diagnosed by computed tomography. For proteomics, tumor samples were obtained from 12 cases at the time of surgery, snap frozen in liquid nitrogen, and stored until use. The adjacent nontumor tissues were also obtained from areas distant from the tumor margin in 8 of these 12 cases. Immunohistochemistry was performed for all 15 ASPS cases including the 12 cases used for proteomics. Clinical information on the 15 patients is detailed in Table 1. Protein contents of the primary tumor tissues were examined in three cases each of gastrointestinal stromal tumor, osteosarcoma, rhabdomyosarcoma, and epithelioid sarcoma (Supplementary Table 1 in the Supporting Information). Protein extracts from normal tissues were obtained from BioChain (Newark, CA). The ASPS cell line ASPS-KY was kindly provided by Dr. Y Miyagi (Kanagawa Cancer Center Research Institute, Kanagawa, Japan). ASPS-KY was cultured in DMEM (supplemented with 10% fetal bovine serum, 1 mmol/L sodium pyruvate, 1 × nonessential amino acids, and 2 mmol/L glutamine) and incubated at 37 °C in a humidified 5% CO_2 atmosphere. This project was approved by the ethical review board of the National Cancer Center, and signed informed consent was obtained from all of the patients included.

Table 1. Summary of Clinicopathological Data of the 15 ASPS Patients

no.	gender	age	location	metastasis
ASPS-1	female	28	femur	none
ASPS-2	female	26	retroperitoneal	recurrence, spleen, bone
ASPS-3	female	23	pelvis	neck, brain
ASPS-4	female	23	buttock	lung
ASPS-5	female	16	femur	lung
ASPS-6	male	35	extremity	bone, lung, brain
ASPS-7	female	29	buttock	lung
ASPS-8	female	14	extremity	none
ASPS-9	male	33	extremity	lung
ASPS-10	female	27	pelvis	lung
ASPS-11	female	33	pelvis	lung
ASPS-12	male	31	femur	lung
ASPS-13	female	47	primary unknown	brain
ASPS-14	female	26	extremity	brain, lung
ASPS-15	female	23	extremity	brain, lung

2.2. Protein Expression Profiling

Proteins were extracted from frozen tissues in accordance with our previous report.[19] In brief, frozen tissues were crushed to powder with a Multibeads shocker (Yasui Kikai, Osaka, Japan) in liquid nitrogen. The frozen powder was then treated with urea lysis buffer (6 M urea, 2 M thiourea, 3% CHAPS, 1% Triton X-100) and centrifuged at 15 000 rpm for 30 min. The supernatant was recovered and stored at −80 °C until use.

Protein expression profiling was performed by 2D-DIGE with our original large-format electrophoresis apparatus.[19] The experiment design for the 2D-DIGE experiments is overviewed in Figure 1A. In brief, the internal standard sample was created by mixing equal portions of all individual samples. Five micrograms each of the internal standard sample and individual sample were labeled with Cy3 and Cy5, respectively (CyDye DIGE Fluor saturation dye, GE, Uppsala, Sweden). These differently labeled protein samples were mixed and separated according to isoelectric point and molecular weight. The first-dimension separation was achieved using Immobiline pH gradient DryStrip gels (24 cm long, pI range 4−7, GE) and Multiphor II (GE). The second-dimension separation was achieved by SDS-PAGE using our original large-format electrophoresis apparatus (33 cm separation distance, Biocraft, Tokyo, Japan).[19] The gels were scanned using laser scanners (Typhoon Trio, GE) at appropriate wavelengths for Cy3 or Cy5 (Figure 1B). For all protein spots, the Cy5 intensity was normalized with the Cy3 intensity in the same gel using the ProgenesisSameSpots software package version 3 (Nonlinear Dynamics, Newcastle-upon-Tyne, U.K.). All samples were examined in triplicate gels, and the mean normalized intensity value was calculated. The experimental reproducibility of 2D-DIGE was examined by running the identical sample three times and evaluating the correlation of the protein spot intensities on a scatter gram (Figure 1C). Mass spectrometric protein identification was performed according to our previous report.[19] In brief, 100 μg of the protein sample was labeled with Cy5 and separated by 2D-PAGE as previously mentioned. Protein spots were recovered from the gels by an automated spot recovery machine (Molecular Hunter, AsOne, Osaka, Japan) and subjected to manual in-gel digestion using trypsin.[19] The tryptic digests were subjected to liquid chromatography coupled with nanoelectrospray tandem mass spectrometry (Finnigan LTQ Orbitrap XL mass spectrometer, Thermo Electron, San Jose, CA). The Mascot software package (version 2.2; Matrix Science, London, U.K.) was used to search for the mass of each peptide ion peak against the SWISS-PROT database (*Homo sapiens*, 471 472 sequences in the Sprot-57.5.fasta file). Proteins with a Mascot score of 34 or more were considered to be positively identified.

2.3. Western Blotting

Five microgram portions of the protein samples were separated by SDS-PAGE (ATTO, Tokyo, Japan). The separated proteins were subsequently blotted on a nitrocellulose membrane and incubated with a monoclonal antibody against SET (1:1000 dilution, Abcam, Cambridge, MA), pAKT(1:500 dilution, BD Bioscience, Franklin Lakes, NJ), Bad (1:500 dilution, BD), Bid (1:500 dilution, BD), and actin (1:5000, Abcam). The membrane was then reacted with horseradish-peroxidase-conjugated secondary antibody (1:3000 dilution, GE), processed using enhanced chemiluminescence reagents (ECL Prime, GE), and scanned with a LAS-3000 laser scanner (FujiFilm, Tokyo, Japan).

2.4. Immunohistochemistry

The most representative areas of tumor and nontumor tissues were sampled for tissue microarray (TMA). The TMAs were assembled with a tissue array instrument (Azumaya, Tokyo, Japan). To reduce sampling bias due to tumor heterogeneity, we used two replicate 2.0-mm-diameter cores from different areas of individual tumors. The TMA consisted of 15 cases of ASPS, including samples from the 12 cases (ASPS1−12) subjected to 2D-DIGE and from 3 newly enrolled cases (ASPS13−15, Table 1).

The expression levels of SET were examined immunohistochemically. In brief, 4-μm-thick formalin-fixed, paraffin-embedded tissue sections and TMAs were autoclaved in 10 mmol/L

dx.doi.org/10.1021/pr400929h | J. Proteome Res. XXXX, XXX, XXX−XXX

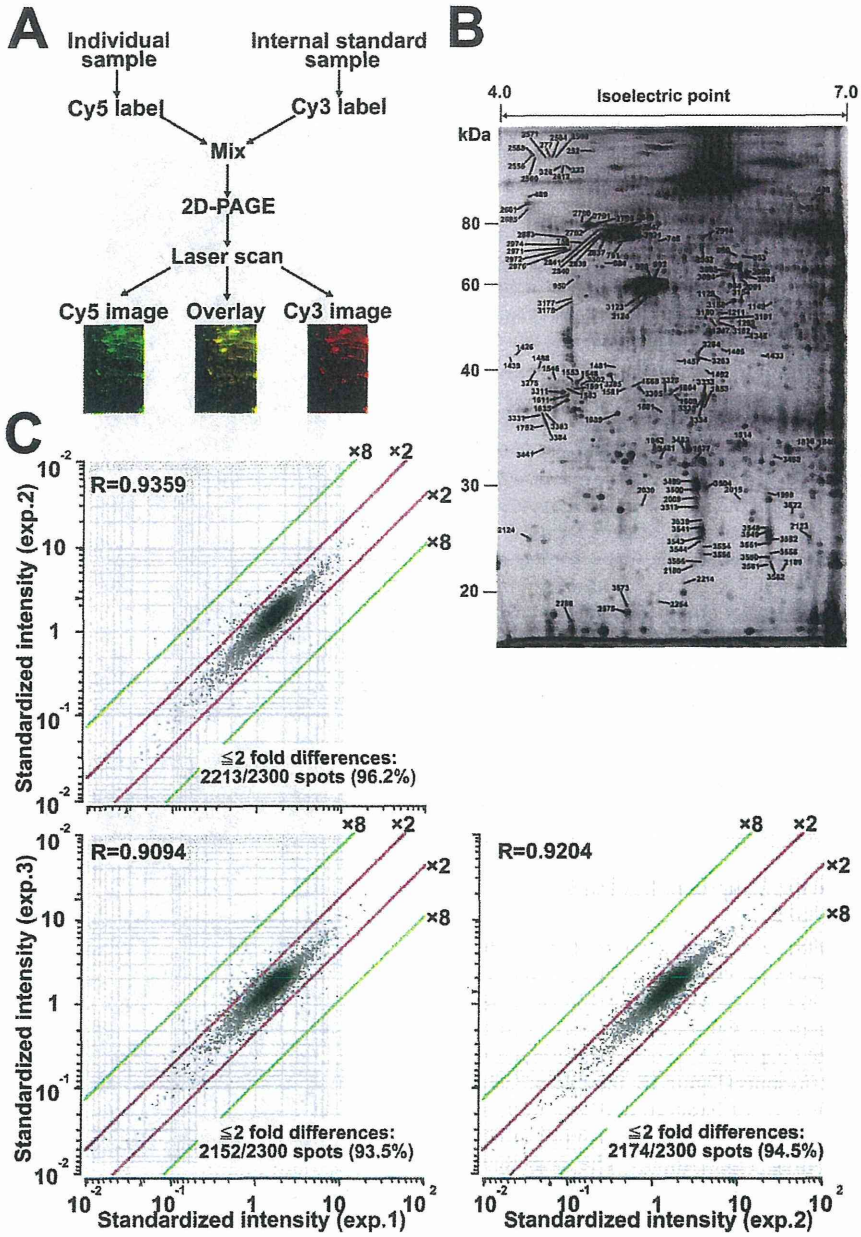

Figure 1. Overview of experiment workflow using 2D-DIGE. (A) Individual samples and internal standard sample were labeled with two different fluorescent dyes, mixed together, and separated by 2D-PAGE. (B) Typical gel image of 2D-DIGE. The protein spot numbers correspond to those in Figure 2, Table 2, and Supplementary Tables 2 and 3 in the Supporting Information. The enlarged image is provided in Supplementary Figure 1 in the Supporting Information. (C) Technical reproducibility was examined by running one identical sample three times. Note that the intensity of at least 93.5% of the protein spots was scattered within a two-fold difference, and the overall correlation coefficient was more than 0.9.

citrate buffer (pH 6.0) at 121 °C for 30 min and incubated with anti-SET antibody (1:500 dilution, Abcam) for 1 h. Immunostaining was carried out by the streptavidin–biotin peroxidase method using an ABC complex/horseradish peroxidase kit (DAKO, Glostrup, Denmark). One pathologist (A.Y.) and one clinician (D.K.) reviewed the stained sections.

2.5. Gene Silencing Assay

SET-specific siRNAs were purchased from Sigma-Aldrich, and control stealth siRNA was from Life Technologies. The target sequences were 5′-rGrCrAUUrAUUUrGrArCrCrArGrArGUUTT-3′ (siRNA-1), 5′-rCrArGrArGUUrGrArArGUrGrArCrArGrArATT-3′ (siRNA-2), and 5′-rGrCrAUUrAUUUrGrArCrCrArGrArGU-UTT –3′ (siRNA-3). A total of 5×10^3 ASPS cells, ASPS-KY, were seeded into each well of a 96-well plate (Coaster, Cambridge, MA). The following day, the cell monolayer was washed with prewarmed sterile phosphate-buffered saline. Cells were transfected with the appropriate siRNA using DharmaFECT transfection reagents (Thermo Fisher, Waltham, MA) in accordance with the manufacturer's protocol. Twenty-four hours later the culture medium for the transfected cells was switched to medium A, whereas the conditioned medium was not changed.

dx.doi.org/10.1021/pr400929h | J. Proteome Res. XXXX, XXX, XXX–XXX

2.6. Cell Proliferation and Invasion Assay

To examine the effects of SET and an inhibitor for PP2A on the ASPS cells, cell proliferation was examined after treatment with siRNAs or a PP2A activator, FTY720 (Selleck Chemicals, Houston, TX). FTY720 was dissolved with dimethyl sulfoxide (DMSO, Wako, Osaka, Japan), and added to the culture medium at an appropriate concentration. Cell proliferation was examined by the tetrazolium-based colorimetric MTT assay. In brief, the cells were transfected with the appropriate siRNA using DharmaFECT transfection reagent for 24 h. Alternatively, the cells were incubated with various concentrations of FTY720. Then, 20 μL of the reagent from Cell Counting Kit-8 (Dojindo, Kumamoto, Japan) was added to each well containing ASPS-KY cells. After 2 h of incubation, the optical density was measured at a wavelength of 450 nm using a microplate reader (SAFARI, TECAN, Männedorf, Switzerland). Cell invasion before and after the treatments was evaluated using the BD BioCoat Invasion Chamber (BD Bioscience) in accordance with the manufacturer's protocol. In brief, the cells were transfected with the appropriate siRNA using DharmaFECT transfection reagent for 24 h. The cells were seeded onto the membrane in the upper chamber of the trans-well at a concentration of 5×10^5 in 500 μL of serum-free medium. The medium in the lower chamber contained 10% fetal calf serum as a source of chemoattractants. Cells that passed through the Matrigel-coated membrane were stained with Diff-Quick (Sysmex, Kobe, Japan), and the cells were counted.

All experiments were performed at least three times, in duplicate or triplicate, and statistical significance was calculated by t test using the SPSS statistical software package (IBM, Armonk, NY).

3. RESULTS

3.1. Protein Expression Profiling Identifies the Set Oncogene Product in ASPS

Protein expression profiles were created by 2D-DIGE, which is advantageous in that gel-to-gel variations can be compensated for by normalizing the expression data for individual samples with those of the common internal standard sample using two different fluorescent dyes (Figure 1A). Such normalization was performed for 2300 protein spots (Figure 1B, the enlarged image is Supplementary Figure 1 in the Supporting Information, and the intensity of all 2300 protein spots is shown in Supplementary Table 2 in the Supporting Information). The large-format electrophoresis apparatus and the internal standard sample resulted in highly reproducible protein expression profiling, as shown by scatter gram for three independent experiments on one identical sample (Figure 1C).

The comparison between tumor and nontumor tissues resulted in the identification of 145 protein spots showing significant differences in intensity (p value less than 0.01 and more than two-fold intensity difference, Figure 2 and Table 2). Mass spectrometry detected the corresponding proteins for these 145 spots. The differential intensities of the protein spots and the results of protein identification are summarized in Figure 2. Detailed data for the identified proteins and supportive data for positive protein identification are provided in Supplementary Table 3 in the Supporting Information.

3.2. Immunological Validation of SET Overexpression in Primary Tumor Tissues of ASPS

We focused in detail on the higher expression of the SET oncogene product. The product of the SET is a multifunctional protein contributing to progression of various cancers and is considered to be a therapeutic target.[20] By Western blotting, we confirmed the overexpression of SET in tumor tissues compared with noncancerous adjacent normal tissues (Figure 3A). SET was observed as a single band with the expected molecular weight (Figure 3A). Immunohistochemistry demonstrated nuclear localization of SET with preferential expression in tumor cells relative to nontumor cells (Figure 3B). We confirmed the overexpression of SET in the 15 cases of ASPS (Supplementary

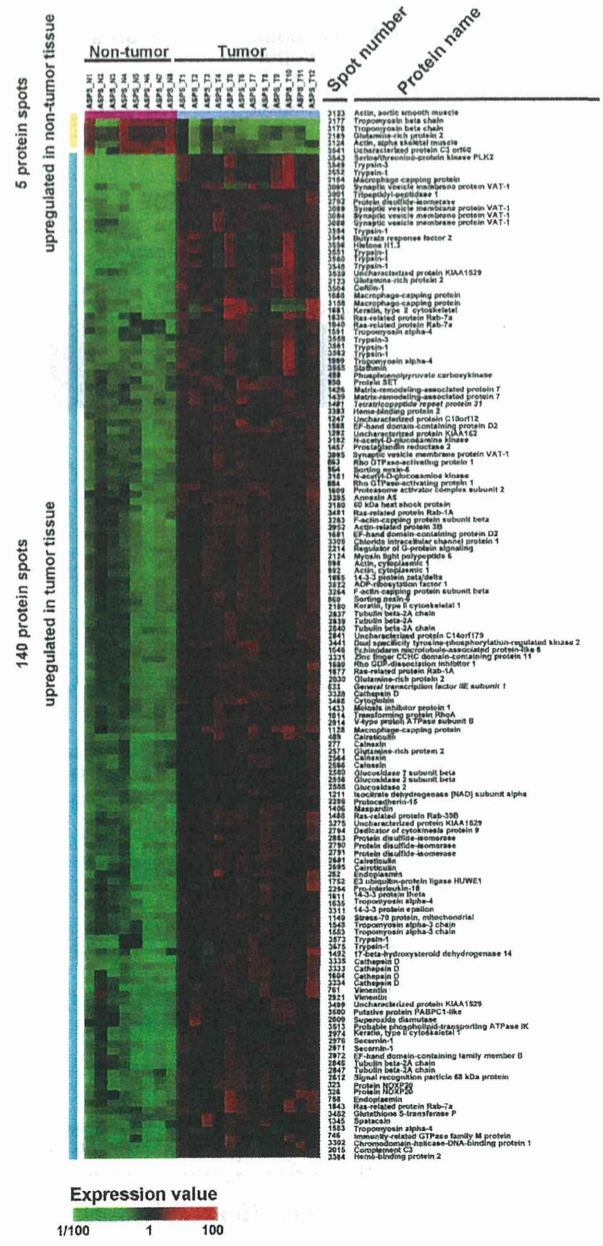

Figure 2. Protein spots with different intensities and their annotation by mass spectrometry. Differences in the intensity of protein spots between tumor tissues and noncancerous adjacent tissues are exhibited in the form of a heat-map. Any intensity showing more than a two-fold difference with statistical significance ($p < 0.05$) was considered to be positive. Mass spectrometry annotation of the protein spots is demonstrated on the right side of the heat-map.

dx.doi.org/10.1021/pr400929h | J. Proteome Res. XXXX, XXX, XXX–XXX

Table 2. Summary of Proteins with Differential Expression between ASPS Tumor Tissues and Nontumor Tissues

spot no.[a]	accession no.[b]	identified protein	Wilcoxon test p value	fold difference (ratio of means)	pI (cal)[c]	MW (cal) (Da)[c]	protein score[d]	peptide matches	sequence coverage (%)
3552	P07477	trypsin-1	1.5877×10^{-5}	0.008515009	6.08	27111	72	1	8.1
3541	Q9P032	uncharacterized protein C3orf60	1.5877×10^{-5}	0.010363941	8.48	20566	67	1	6
3549	P35030	trypsin-3	1.5877×10^{-5}	0.010390875	7.46	33306	58	1	4.3
3543	Q9NYY3	serine/threonine-protein kinase PLK2	1.5877×10^{-5}	0.011751306	8.52	79270	37	1	1.3
3089	Q99536	synaptic vesicle membrane protein VAT-1	1.5877×10^{-5}	0.021958413	5.88	42122	185	2	8.9
3091	O14773	tripeptidyl-peptidase 1	1.5877×10^{-5}	0.02956955	6.01	61723	149	3	8.2
3539	Q9P1Z9	uncharacterized protein KIAA1529	1.5877×10^{-5}	0.029933118	5.74	192404	40	1	1.2
2792	P07237	protein disulfide-isomerase	1.5877×10^{-5}	0.03101972	4.76	57480	1138	38	35.8
3551	P07477	trypsin-1	1.5877×10^{-5}	0.031037268	6.08	27111	43	1	8.1
3335	P07339	cathepsin D	1.5877×10^{-5}	0.032525296	6.1	45037	254	4	14.3
3090	Q99536	synaptic vesicle membrane protein VAT-1	1.5877×10^{-5}	0.034147549	5.88	42122	225	5	21.4
3556	P16402	histone H1.3	1.5877×10^{-5}	0.035355776	11	22336	32	1	4.1
3544	P47974	butyrate response factor 2	1.5877×10^{-5}	0.036972559	8.52	52000	38	1	5.1
3154	P40121	macrophage-capping protein	3.1754×10^{-5}	0.037782583	5.88	38779	429	8	26.1
2123	Q9H0J4	glutamine-rich protein 2	1.5877×10^{-5}	0.039776539	6.25	181228	42	1	0.5
3560	P07477	trypsin-1	1.5877×10^{-5}	0.041918698	6.08	27111	63	1	8.1
3554	P07477	trypsin-1	1.5877×10^{-5}	0.043031618	6.08	27111	58	1	8.1
3084	Q99536	synaptic vesicle membrane protein VAT-1	1.5877×10^{-5}	0.043691971	5.88	42122	356	7	19.8
3088	Q99536	synaptic vesicle membrane protein VAT-1	1.5877×10^{-5}	0.044704717	5.88	42122	215	5	12.5
3158	P40121	macrophage-capping protein	0.00011114	0.04492316	5.88	38779	332	9	21.8
3504	P23528	cofilin-1	1.5877×10^{-5}	0.046486714	8.22	18719	53	1	6.6
3548	P07477	trypsin-1	1.5877×10^{-5}	0.051111972	6.08	27111	79	1	8.1
1604	P07339	cathepsin D	1.5877×10^{-5}	0.052422591	6.1	45037	91	2	6.3
2015	P01024	complement C3	1.5877×10^{-5}	0.053827382	6.02	188569	58	1	1.3
1488	Q96DA2	Ras-related protein Rab-39B	1.5877×10^{-5}	0.054075741	7.7	24835	36	1	6.1
2791	P07237	protein disulfide-isomerase	1.5877×10^{-5}	0.056152907	4.76	57480	71	2	4.7
2681	P27797	calreticulin	1.5877×10^{-5}	0.059656716	4.29	48283	504	14	26.6
489	P27797	calreticulin	1.5877×10^{-5}	0.059974668	4.29	48283	94	2	4.3
3333	P07339	cathepsin D	1.5877×10^{-5}	0.060978434	6.1	45037	153	4	11.2
3558	P35030	trypsin-3	1.5877×10^{-5}	0.062680878	7.46	33306	60	1	4.3
2976	Q12765	secernin-1	1.5877×10^{-5}	0.062850066	4.66	46980	86	2	6.3
2883	Q6ZMW3	echinoderm microtubule-associated protein-like 6	1.5877×10^{-5}	0.062965523	7.17	220270	50	2	0.4
761	P08670	vimentin	0.0004763	0.065528927	5.06	53676	358	15	23.6
3384	Q9Y5Z4	heme-binding protein 2	1.5877×10^{-5}	0.067161156	4.58	22861	143	2	13.2
1406	Q9NZD8	maspardin	1.5877×10^{-5}	0.068166	5.85	35223	82	1	3.9
3499	Q9P1Z9	uncharacterized protein KIAA1529	1.5877×10^{-5}	0.068985159	5.74	192404	43	1	1.2
1568	Q96C19	EF-hand domain-containing protein D2	1.5877×10^{-5}	0.071337515	5.15	26794	165	3	15
1611	P27348	14-3-3 protein theta	1.5877×10^{-5}	0.074204821	4.68	28032	74	1	5.7
2974	P04264	keratin, type II cytoskeletal 1	1.5877×10^{-5}	0.074765405	8.15	66170	122	2	3.7
3500	P11940	putative protein PABPC1-like	1.5877×10^{-5}	0.075151195	8.88	30256	49	1	7.4
3302	O14646	chromodomain-helicase-DNA-binding protein 1	1.5877×10^{-5}	0.075335702	6.72	197538	40	1	0.5
3562	P07477	trypsin-1	1.5877×10^{-5}	0.076824606	6.08	27111	63	1	8.1
3275	Q9P1Z9	uncharacterized protein KIAA1529	1.5877×10^{-5}	0.07718673	5.74	192404	42	3	1.2
1752	Q7Z6Z7	E3 ubiquitin-protein ligase HUWE1	1.5877×10^{-5}	0.079027202	5.1	485523	39	1	0.3
2846	Q13885	tubulin beta-2A chain	1.5877×10^{-5}	0.079394824	4.78	50274	975	18	43.8
1686	P40121	macrophage-capping protein	1.5877×10^{-5}	0.079825987	5.88	38779	154	4	8.3
3334	P07339	cathepsin D	1.5877×10^{-5}	0.079953736	6.1	45037	310	6	16.5
323	Q8IWE2	protein NOXP20	1.5877×10^{-5}	0.080187134	4.61	61046	267	6	15.1
2558	P14314	glucosidase 2 subunit beta	1.5877×10^{-5}	0.080715302	4.33	60357	316	5	10.6
2794	P07237	protein disulfide-isomerase	1.5877×10^{-5}	0.081241738	4.76	57480	841	25	32.5
326	Q8IWE2	protein NOXP20	1.5877×10^{-5}	0.081614914	4.61	61046	82	2	3.7
2695	P27797	calreticulin	1.5877×10^{-5}	0.083690191	4.29	48283	209	4	9.4
3575	P07477	trypsin-1	0.00019052	0.083697415	6.08	27111	61	1	8.1
3182	Q9UJ70	*N*-acetyl-D-glucosamine kinase	1.5877×10^{-5}	0.084723353	5.81	37694	388	6	25

dx.doi.org/10.1021/pr400929h | J. Proteome Res. XXXX, XXX, XXX–XXX